NEURODEVELOPMENT

Distinct molecular programs regulate synapse specificity in cortical inhibitory circuits

Emilia Favuzzi[1,2,3]*, Rubén Deogracias[1,2,3]*, André Marques-Smith[1,2], Patricia Maeso[1,2,3], Julie Jezequel[1,2], David Exposito-Alonso[1,2], Maddalena Balia[1,2], Tim Kroon[1,2], Antonio J. Hinojosa[1,2,3], Elisa F. Maraver[1,2], Beatriz Rico[1,2,3]†

How neuronal connections are established and organized into functional networks determines brain function. In the mammalian cerebral cortex, different classes of GABAergic interneurons exhibit specific connectivity patterns that underlie their ability to shape temporal dynamics and information processing. Much progress has been made toward parsing interneuron diversity, yet the molecular mechanisms by which interneuron-specific connectivity motifs emerge remain unclear. In this study, we investigated transcriptional dynamics in different classes of interneurons during the formation of cortical inhibitory circuits in mouse. We found that whether interneurons form synapses on the dendrites, soma, or axon initial segment of pyramidal cells is determined by synaptic molecules that are expressed in a subtype-specific manner. Thus, cell-specific molecular programs that unfold during early postnatal development underlie the connectivity patterns of cortical interneurons.

Different classes of neurons connect with exquisite specificity to form neuronal circuitries. Brain wiring is most complex in the cerebral cortex, which contains excitatory pyramidal cells and inhibitory GABAergic interneurons, of which more than two dozen types have been identified (*1*). Different types of interneurons target distinct subcellular compartments in pyramidal cells. For example, somatostatin-expressing (SST+) interneurons primarily contact the dendrites of pyramidal cells, whereas parvalbumin-expressing (PV+) basket cells make synapses on neuronal somata and proximal dendrites. Chandelier cells, on the other hand, innervate the axonal initial segment (AIS) of pyramidal neurons (*2*). Compartment-specific inhibitory control confers advanced computational capabilities to neurons (*3*, *4*). In this work, we studied the mechanisms regulating compartment-specific wiring of interneuron outputs in cortical microcircuits in mouse. Molecular signatures identify types of interneurons in the adult mouse cerebral cortex (*1*, *5*, *6*). However, cell type–specific transcriptional differences may drive subcellular patterns of inhibitory connectivity and may be restricted to early postnatal development, when synapses are formed.

To identify cell type–specific molecular programs controlling the subcellular connectivity of SST+, PV+ basket, and chandelier interneurons, we first analyzed the temporal dynamics of inhibitory synapse formation for each of these populations (fig. S1). Postnatal day 10 (P10) marks the initial surge of synaptogenesis for all three classes of interneurons (fig. S1). These results provided us with a developmental time window for searching gene expression differences underlying the establishment of type-specific interneuron connectivity.

To identify genes that are differentially expressed between different classes of interneurons during inhibitory synapse formation, we used fluorescence-activated cell sorting to isolate interneurons from genetically modified mice in which dendritic-, somatic-, and AIS-targeting GABAergic interneurons are enriched and labeled (table S1) (*7*–*12*). We isolated interneurons both before (P5 or P8) and during peak (P10) synaptogenesis. To ensure cell type and developmental stage specificity, we also isolated several control populations: interneurons at P0, pyramidal neurons at the peak of glutamatergic synaptogenesis (P12) (*13*), and oligodendrocytes at P10 (tables S1 and S2). We then performed RNA-sequencing (RNA-seq) and whole-transcriptome analyses on each of these cell populations to identify the molecular programs that distinguish different interneuron types between P5 and P10 (Fig. 1A and fig. S2A) (https://devneuro.org/cdn/synapdomain.php). Gene expression profiles from different types of interneurons showed similar patterns of distribution, consistency across biological replicates, accurate segregation for each cell type, and suitability of the selected developmental time points (fig. S2).

To determine which molecules regulate interneuron synapse specificity, we first identified differentially expressed (DE) genes among distinct types of interneurons during the initial period of synaptogenesis (Fig. 1). Differential expression analysis revealed type-specific gene expression at P10 (Fig. 1B and fig. S3C). Gene Ontology (GO) analysis revealed that the most enriched genes belong to synaptic, nearby membrane compartments and include processes that contribute to synaptogenesis (Fig. 1, C and D, and fig. S3). Notably, comparison of our dataset with recent single-cell RNA-seq studies from the adult mouse cortex revealed that many genes that are type-specific during development are not detected as such at later stages in mature brains (figs. S4 to S6). Altogether, these analyses indicate that distinct transcriptomic profiles emerge in developing interneurons and that a large proportion of the type-specific signatures are restricted to the time of synapse assembly (P5 to P10).

To single out genes with the highest degree of type and stage specificity, we ranked DE genes using a specificity ratio (*14*) (see supplementary methods). Our analyses (i) indicate that different interneurons acquire distinct molecular signatures when they first establish synaptic contacts (Fig. 1E) and (ii) reveal several gene subsets potentially involved in the establishment of distinct (dendrite-, soma-, and AIS-targeting) inhibitory motifs in the developing cerebral cortex (Fig. 2A, fig. S7, and tables S3 and S4). Indeed, our data showed that distinct members of synaptic protein families are often differentially used by interneuron subclasses during development (Fig. 2B and fig. S8). Focusing on genes that had a putative or established synaptic function (Fig. 2, A and B), we identified and validated those that exhibited the highest specificity (Fig. 2 and figs. S9 and S10). Such validation yielded three candidate genes that we further studied to demonstrate that inhibitory synapse specificity is conferred by cell-specific expression of synaptic molecules. The leading candidate for regulating dendrite-targeting inhibitory synapses was *Cbln4*, a member of the C1q family that is a bidirectional synaptic organizer (*15*, *16*). Leucine-rich repeat LGI family member 2 (*Lgi2*), which belongs to a protein family involved in synapse maturation (*17*), emerged as a promising candidate to regulate the development of perisomatic inhibitory synapses. Finally, *Fgf13*, which encodes an intracellular protein with multiple functions, including a microtubule stabilizing role (*18*–*21*), was our candidate for AIS-targeting chandelier synapses. Supporting our hypothesis that these genes aid inhibitory synapse development, *Lgi2* and *Fgf13* dysfunction has been linked to disorders characterized by disrupted excitatory/inhibitory balance (*22*–*24*).

We examined mRNA or protein expression for our candidate genes and confirmed that their expression increased during the second postnatal week (Fig. 2C). We also confirmed that in the cerebral cortex, both at P10 and P30, *Cbln4*, *Lgi2*, and *Fgf13* are enriched in SST+, PV+ basket, and chandelier cells, respectively (Fig. 2, D and E, and figs. S10 and S11). Examining the proportion of interneurons of each type that express our candidate genes, one can see that *Cbln4* and *Fgf13* are ubiquitously expressed

[1]Centre for Developmental Neurobiology, Institute of Psychiatry, Psychology and Neuroscience, King's College London, London SE1 1UL, UK. [2]MRC Centre for Neurodevelopmental Disorders, King's College London, London SE1 1UL, UK. [3]Instituto de Neurociencias, Consejo Superior de Investigaciones Científicas–Universidad Miguel Hernández, Sant Joan d'Alacant 03550, Spain.
*These authors contributed equally to this work.
†Corresponding author. Email: beatriz.rico@kcl.ac.uk

by all SST+ interneurons and chandelier cells, respectively, whereas *Lgi2* is confined to a subpopulation of PV+ basket cells (Fig. 2, D and E, and fig. S10).

To investigate the role of *Cbln4*, *Lgi2*, and *Fgf13* in the development of different types of GABAergic synapses, we used a hybrid conditional gene knockdown strategy based on cell type–specific Cre-driver lines combined with adeno-associated virus (AAV) vectors and performed cell type–specific loss-of-function experiments in vivo (*25*). In brief, we engineered Cre-dependent conditional constructs expressing miR-based short-hairpin RNAs against candidate genes (*shCbln4*, *shLgi2*, and *shFgf13*) and controls (*shLacZ* and *shGfp*) in which recombination was reported by mCherry labeling (fig. S12A). We confirmed the effectiveness of our constructs in down-regulating *Cbln4*, *Lgi2*, and *Fgf13* expression (fig. S12, B to E).

Compared with controls, cell-specific down-regulation of *Cbln4* in SST+ cells, *Lgi2* in PV+ basket cells, and *Fgf13* in chandelier cells led to a decrease in the density of presynaptic inputs

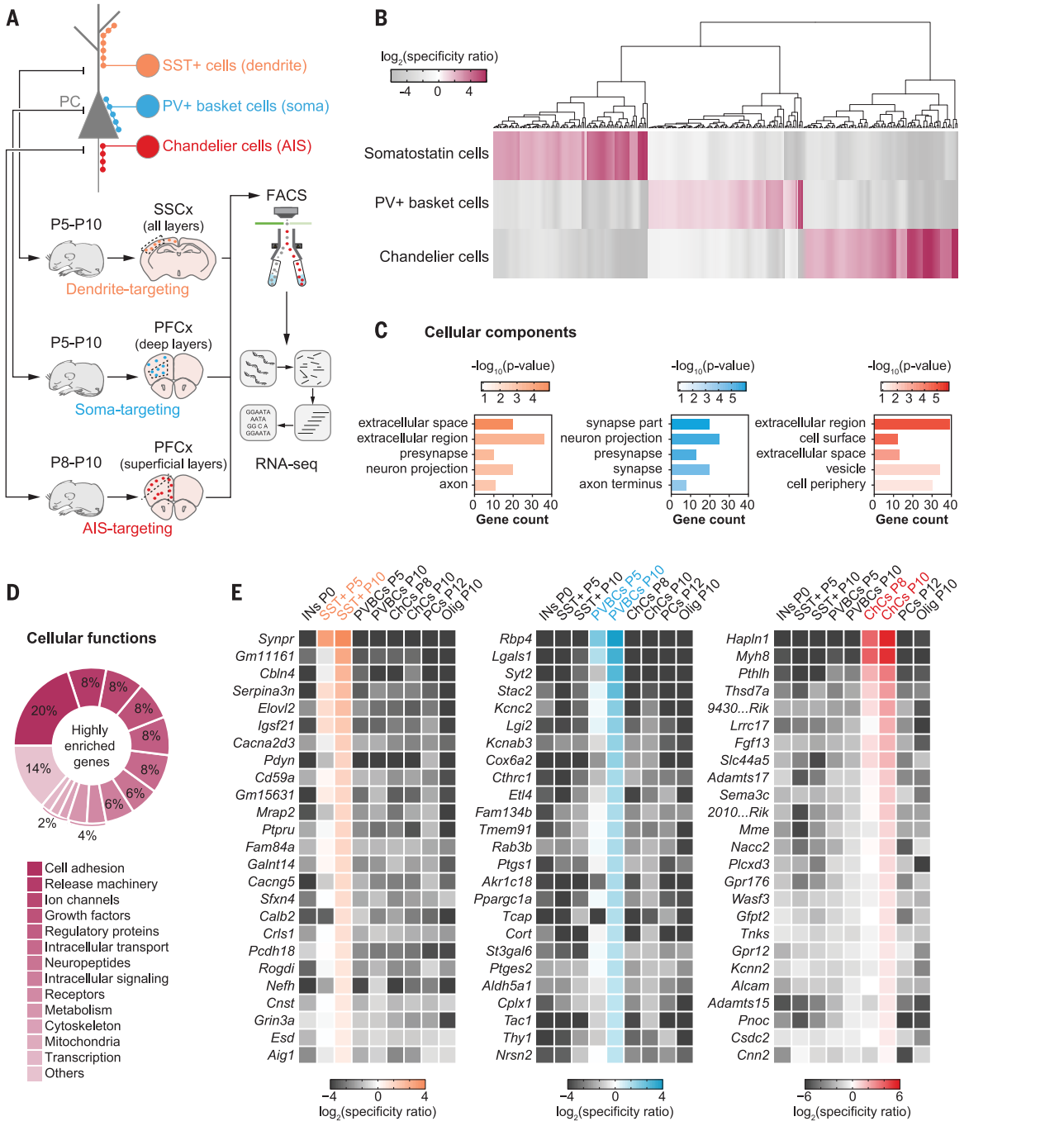

Fig. 1. Identification of cell type–specific molecular programs for postnatal development of interneurons. (**A**) Schematic of experimental workflow. PC, pyramidal cell; SSCx, somatosensory cortex; PFCx, prefrontal cortex; FACS, fluorescence-activated cell sorting. (**B**) Heatmap showing P10 interneuron-subtype enriched genes. (**C** and **D**) GO analysis using P10 subtype-specific genes: terms associated with synapses (C) (fig. S3) and cellular functions (D). (**E**) Heatmaps showing the top 25 DE genes exhibiting the highest degree of subtype and stage specificity. INs, interneurons; SST+, somatostatin-expressing cells (SST+); PVBCs, parvalbumin-expressing (PV+) basket cells; ChCs, chandelier cells; Olig, oligodendrocytes.

(mCherry+) that these interneurons make onto the corresponding subcellular postsynaptic compartments of pyramidal cells (Fig. 3 and fig. S13). We observed that *Fgf13*-deficient chandelier cells also showed axonal disorganization (fig. S14, A to D), which was not found in SST+ or PV+ basket cells upon down-regulation of *Cbln4* and *Lgi2*, respectively (fig. S15). The axonal phenotype of *Fgf13*-deficient chandelier cells may contribute to their decreased innervation of the AIS. Nevertheless, the reduced density of chandelier synaptic boutons persisted when *Fgf13* was down-regulated after P14, and the axonal phenotype was, instead, not observed (fig. S14, E to H), suggesting two different functions of the protein.

Control as well as rescue experiments showed that our phenotypes are explained by specific down-regulation of the target genes rather than off-target effects and do not include an altered interneuron density (figs. S16 to S18). Moreover, GluD1 and ADAM22—CBLN4 and LGI2 putative transsynaptic partners (*23*, *26*)—are located at the SST+ and PV+ basket synapses, respectively (fig. S19).

Altogether, these experiments revealed that *Cbln4*, *Lgi2*, and *Fgf13* are required for the development of dendrite-, soma-, and AIS-targeting synapses made by SST+ interneurons, PV+ basket cells, and chandelier cells, respectively. Such one-to-one matching of molecules to cell types shows that the connectivity patterns of cortical interneurons rely on synaptic protein repertoires that are selective for each type of interneuron. Notably, Cre-dependent knockdown of *Pcdh18*—another developmentally regulated molecule specifically expressed in SST+ cells (Fig. 2A and fig. S20, A to F)—led to an increase in the density of SST+ dendritic synapses (fig. S20, G to J). Thus, our screening is a valuable resource for identifying molecules regulating diverse aspects of inhibitory synapse assembly and specificity.

The subcellular localization of presynapses defines the efferent specificity in each type of interneuron. Therefore, we asked whether the identified cell-specific synaptic molecules can regulate synapse formation independently of the subcellular location of presynaptic terminals. To this end, we focused on *Cbln4* because C1q family proteins can induce synapse formation (*16*). We first validated the synaptic deficits observed after loss of *Cbln4* in SST+ interneurons. Specifically, we injected AAV expressing channelrhodopsin-2 (Chronos) after Cre-mediated recombination along with control or *shCbln4* vectors (Fig. 4A). *Cbln4* down-regulation in SST+ interneurons did not affect their spiking output or membrane properties in response to photostimulation (fig. S21). We recorded from pyramidal neurons and stimulated ChR2+ SST cells with wide-field illumination of increasing intensity, finding that the peak amplitude of optogenetically-evoked inhibitory postsynaptic currents (IPSCs) was reduced in knockdown animals versus controls (Fig. 4, B to D). Minimal intensity stimulation experiments revealed a decrease in IPSC amplitude in cells recorded from knockdown

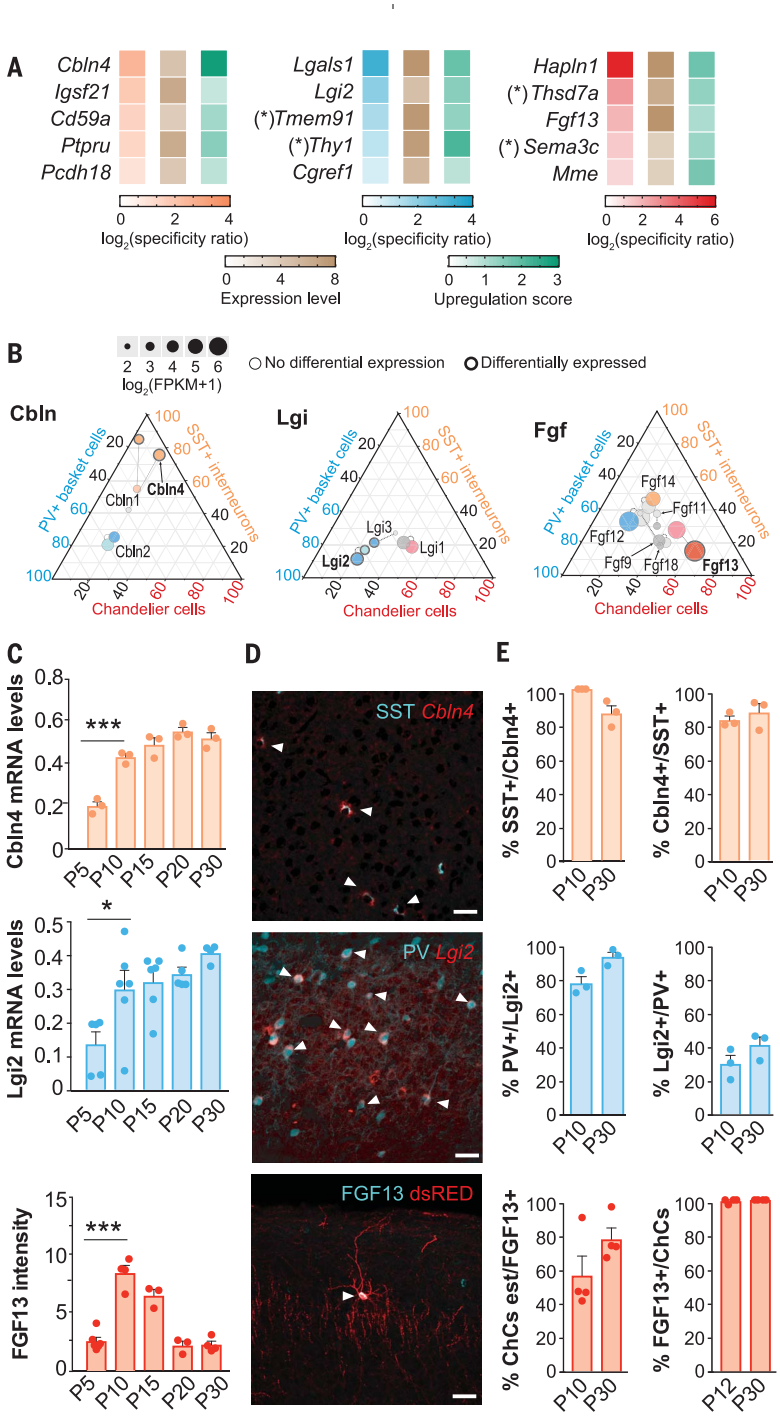

Fig. 2. Expression of subtype-specific synaptic genes. (**A**) Top five candidate subtype-specific synaptic genes. Asterisks indicate synaptic function inferred from similar or related genes. (**B**) Ternary diagrams showing subtype and time differences in expression (light colors, P5; darker colors, P10; gray, not enriched). FPKM, fragments per kilobase of transcript per million fragments mapped. (**C**) Developmental expression of *Cbln4* and *Lgi2* in the somatosensory cortex (quantitative polymerase chain reaction; *Lgi2* values are $\times 10^{-5}$) and FGF13 (IHC, fluorescence intensity in arbitrary units $\times 10^{-2}$) in layers II-III of prefrontal cortex ($n \geq 3$ mice for each stage). One-way analysis of variance (ANOVA) (*Cbln4* and FGF13) or Kruskal-Wallis test (*Lgi2*) and Tukey's or Dunn's multiple comparisons test. $^{***}P < 0.001$, $^{*}P < 0.05$; significance shown only for P5 to P10 comparisons. (**D**) Expression of *Cbln4*, *Lgi2*, and FGF13 in SST+, PV+ basket, and chandelier cells, respectively. White arrowheads indicate colocalization. Scale bars, 20 μm. (**E**) Specificity of *Cbln4*, *Lgi2*, and FGF13 expression (left column). Fraction of SST+, PV+ basket, and chandelier cells expressing *Cbln4*, *Lgi2*, and FGF13 (right column). ChCs est, estimated number of chandelier cells (fig. S4, E to G). Data are mean ± SEM.

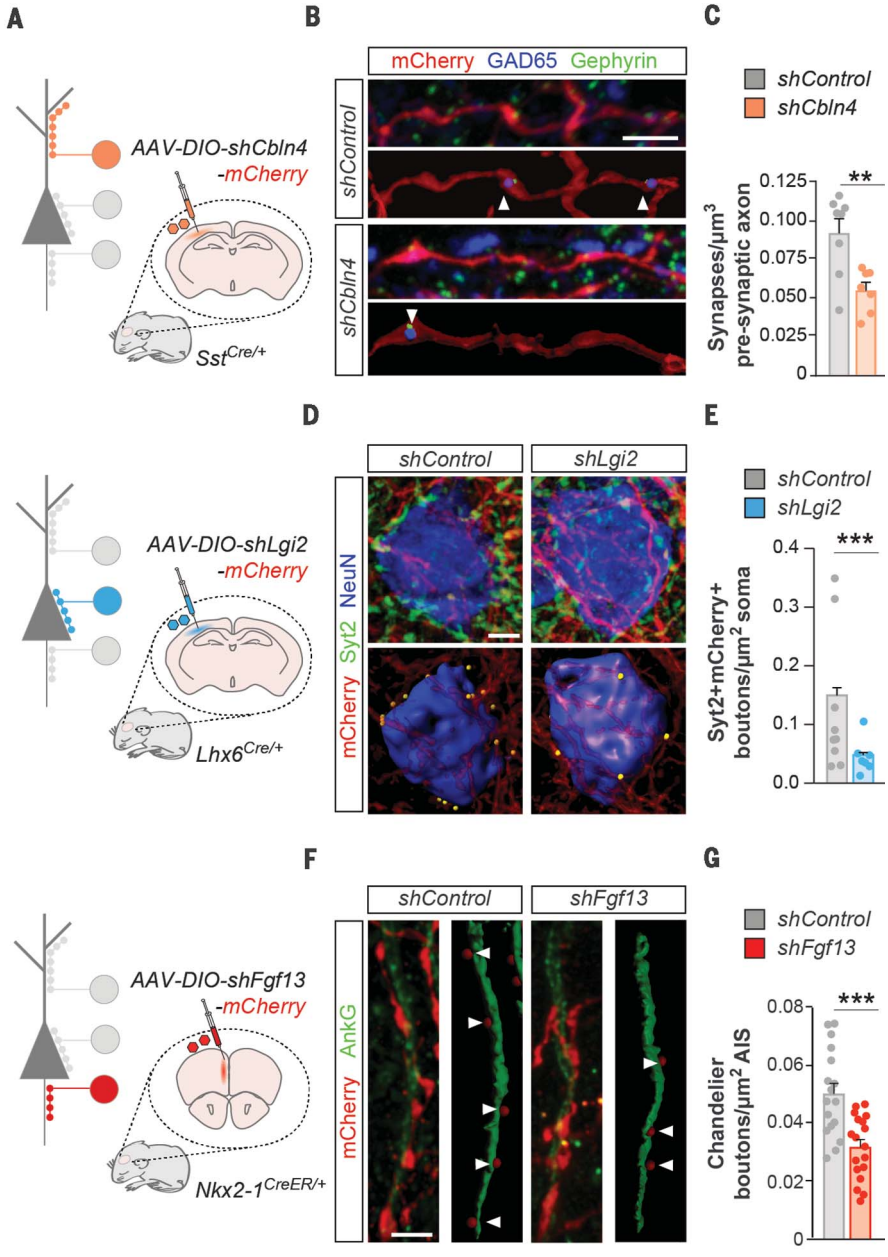

Fig. 3. Genetic specification of interneuron synapse formation. (**A**) Schematic of AAV driving double-floxed invert orientation (DIO) plasmid injections. (**B**) Representative images (top) and Imaris reconstruction (bottom) and (**C**) density of GAD65+ boutons inside mCherry+ axons of SST+ cells infected with control (n = 8 mice) or *shCbln4*-expressing viruses (n = 7 mice) contacting Gephyrin+ clusters in layer I. $^{**}P < 0.01$, Student's t test. (**D**) Representative images (top) and Imaris reconstruction (bottom) and (**E**) density of mCherry+Syt2+ synapses made by PV+ basket cells infected with control (n = 265 cells from 9 mice) or *shLgi2*-expressing virus (n = 136 cells from 7 mice). $^{***}P < 0.0001$, Student's t test. (**F**) Representative images (left) and Imaris reconstruction (right) and (**G**) density of mCherry+ synapses made by chandelier cells induced with tamoxifen and infected with control (n = 18 cells from 3 mice) or *shFgf13*-expressing viruses (n = 18 cells from 5 mice). $^{***}P < 0.001$, Student's t test. White arrowheads indicate colocalization. Scale bars, 1 µm. Data are mean ± SEM.

animals (Fig. 4D). These findings suggest a decrease in synaptic weights for SST outputs to pyramidal cells, offering a functional correlate consistent with the structural synaptic deficits caused by down-regulation of *Cbln4* in SST+ cells (Fig. 3, B and C).

Next, we investigated whether *Cbln4* is sufficient to trigger the formation of domain-restricted synapses. We observed that overexpression of a hemagglutinin (HA)–tagged *Cbln4* in SST+ interneurons leads to an increase in dendritic inhibitory synapses (Fig. 4, E and F). In contrast, ectopic expression of CBLN4 in PV+ basket cells or chandelier cells did not promote synapse formation on the soma or AIS of pyramidal cells but caused a specific increase in PV+ dendritic synapses (Fig. 4, G to L, and fig. S22). These results indicate that *Cbln4* expression does not trigger generic formation of all inhibitory synapses. Rather, *Cbln4* promotes the formation of GABAergic synapses onto the dendrites of pyramidal cells, a feature that is distinctive of SST+ interneurons.

Our study reveals transcriptional dynamics for different classes of interneurons from P5 to P10 in postnatal development of the mouse, when inhibitory circuits are established in the cerebral cortex. Although posttranscriptional processes (e.g., local translation) are likely to play an additional role, our results describe a relationship between cortical interneuron development and diversity. We demonstrate that different classes of interneurons rely on largely nonoverlapping molecular programs for the establishment of distinct types of inhibitory synapses. In particular, we show that three molecules—CBLN4, LGI2, and FGF13—regulate the development of SST+, PV+ basket, and chandelier synapses, respectively. Specifically, CBLN4 is able to promote the assembly of dendritic but not somatic or axo-axonic inhibitory synapses. These results demonstrate how the cell-specific expression of synaptic molecules, together with their ability to promote compartment-specific synapse formation, critically contributes to the specific wiring of the inhibitory circuits.

Insight into the organizing principles of cortical inhibitory circuits will help to decipher neurodevelopmental disorders linked to inhibitory circuit dysfunction (*24*, *27*). Much progress has been made toward understanding interneuron diversity during embryonic development and in the adult cortex (*1*, *6*, *28*–*30*). Our work reveals that selective type-specific genetic programs emerge

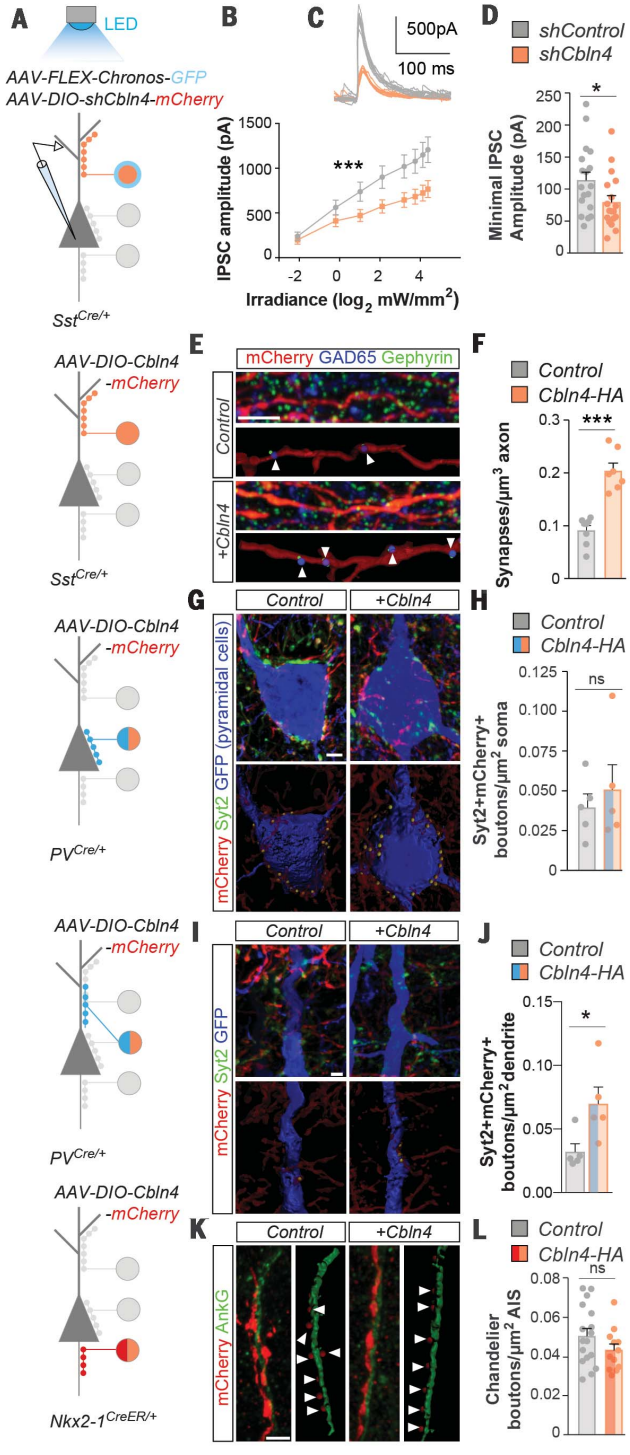

Fig. 4. Synaptic function and target specificity for SST population. (**A**) Schematic of experimental paradigm (n = 18 cells from 9 and 7 mice for control and *shCbln4*-expressing viruses, respectively). LED, light-emitting diode; GFP, green fluorescent protein. (**B**) IPSC peak amplitude as a function of irradiance, ***P < 0.001, two-way ANOVA. (**C**) Representative IPSC traces. (**D**) IPSC amplitude under minimal intensity, *P < 0.05, Mann-Whitney test. (**E**) Representative images (top) and Imaris reconstruction (bottom) and (**F**) density of GAD65+ boutons inside mCherry+ axons of SST+ cells infected with control (n = 9 mice) or *Cbln4*-HA–expressing virus (n = 8 mice) contacting Gephyrin+ clusters in layer I. ***P < 0.001, Mann-Whitney test. (**G** and **I**) Representative images (top) and Imaris reconstruction (bottom) and (**H** and **J**) density of mCherry+Syt2+ synapses made onto pyramidal cell soma [(G) and (H)] or dendrites [(I) and (J)] by PV+ basket cells infected with control (n = 5 mice) or *Cbln4*-HA–expressing virus (n = 5 mice). (H) ns, not significant; Student's t test. (J) *P < 0.05, Mann-Whitney test. (**K**) Representative images (left) and Imaris reconstruction (right) and (**L**) density of mCherry+ synapses made by chandelier cells induced with tamoxifen and infected with control (n = 12 cells from 3 mice) or *Cbln4*-HA–expressing virus (n = 17 cells from 5 mice). Student's t test. White arrowheads indicate colocalization. Scale bars, 1 µm. Data are mean ± SEM.

during postnatal development in cortical interneurons to support the exquisite precision of inhibitory connections, thereby assembling inhibitory circuits. Because some of these genes continue to be expressed in mature cortical interneurons (*1, 5, 6*), it is conceivable that they also contribute to the maintenance and plasticity of specific inhibitory circuitries.

REFERENCES AND NOTES

1. B. Tasic *et al.*, *Nat. Neurosci.* **19**, 335–346 (2016).
2. R. Tremblay, S. Lee, B. Rudy, *Neuron* **91**, 260–292 (2016).
3. F. Pouille, M. Scanziani, *Science* **293**, 1159–1163 (2001).
4. X. J. Wang, J. Tegnér, C. Constantinidis, P. S. Goldman-Rakic, *Proc. Natl. Acad. Sci. U.S.A.* **101**, 1368–1373 (2004).
5. A. Zeisel *et al.*, *Science* **347**, 1138–1142 (2015).
6. A. Paul *et al.*, *Cell* **171**, 522–539.e20 (2017).
7. B. Chattopadhyaya *et al.*, *J. Neurosci.* **24**, 9598–9611 (2004).
8. A. A. Oliva Jr., M. Jiang, T. Lam, K. L. Smith, J. W. Swann, *J. Neurosci.* **20**, 3354–3368 (2000).
9. H. Taniguchi, J. Lu, Z. J. Huang, *Science* **339**, 70–74 (2013).
10. K. Sugino *et al.*, *Nat. Neurosci.* **9**, 99–107 (2006).
11. X. Xu, E. M. Callaway, *J. Neurosci.* **29**, 70–85 (2009).
12. J.-M. Yang *et al.*, *J. Neurosci.* **33**, 19724–19733 (2013).
13. A. J. Hinojosa, R. Deogracias, B. Rico, *Cell Rep.* **24**, 1231–1242 (2018).
14. S. Siegert *et al.*, *Nat. Neurosci.* **15**, 487–495 (2012).
15. M. Yuzaki, *Eur. J. Neurosci.* **32**, 191–197 (2010).
16. M. Yuzaki, *Curr. Opin. Neurobiol.* **45**, 9–15 (2017).
17. K. L. Lovero, Y. Fukata, A. J. Granger, M. Fukata, R. A. Nicoll, *Proc. Natl. Acad. Sci. U.S.A.* **112**, E4129–E4137 (2015).
18. M. Goldfarb *et al.*, *Neuron* **55**, 449–463 (2007).
19. J. L. Pablo, C. Wang, M. M. Presby, G. S. Pitt, *Proc. Natl. Acad. Sci. U.S.A.* **113**, E2665–E2674 (2016).
20. L. Yang *et al.*, *Neuron* **93**, 806–821.e9 (2017).
21. Q.-F. Wu *et al.*, *Cell* **149**, 1549–1564 (2012).
22. R. S. Puranam *et al.*, *J. Neurosci.* **35**, 8866–8881 (2015).
23. E. H. Seppälä *et al.*, *PLOS Genet.* **7**, e1002194 (2011).
24. O. Marín, *Nat. Med.* **22**, 1229–1238 (2016).
25. E. Favuzzi *et al.*, *Neuron* **95**, 639–655.e10 (2017).
26. M. Yasumura *et al.*, *J. Neurochem.* **121**, 705–716 (2012).
27. J. T. Paz, J. R. Huguenard, *Nat. Neurosci.* **18**, 351–359 (2015).
28. X. Jiang *et al.*, *Science* **350**, aac9462 (2015).
29. D. Mi *et al.*, *Science* **360**, 81–85 (2018).
30. C. Mayer *et al.*, *Nature* **555**, 457–462 (2018).

ACKNOWLEDGMENTS

We thank N. Carvajal, L. Doglio, D. Baeza, and I. Andrew for lab support; L. Lim for in utero injections; S. Arber, N. Kessaris, B. Zalc, J. Huang, S. A. Anderson, S. Goebbels, and K. Nave for mouse lines; L. Tricoire for GluD1 antibody; CRG Genomic and Bioinformatic facilities for RNA-seq; and G. Wray for the Synapdomain website. We thank O. Marín and G. Fishell for critical reading of the manuscript, and members of the Flames, Marín, and Rico laboratories for discussions and ideas. **Funding:** Supported by grants from the European Research Council (ERC-2012-StG 310021) and Wellcome Trust (202758/Z/16/Z) to B.R. E.F. was a JAE-Pre fellow (CSIC). B.R. is a Wellcome Trust Investigator. **Author contributions:** E.F. and B.R. managed the study; E.F., R.D., A.M.-S., and B.R. designed the experiments; E.F., P.M., R.D., and A.M.-S. performed the experiments; E.F., J.J., A.M.-S., D.E.-A., and R.D. performed analyses; M.B. and T.K. contributed to quantifications; E.F.M. conducted morphological analyses; A.J.H. contributed with pyramidal cell microarray data; B.R. acquired funding; and E.F. and B.R. wrote the manuscript. **Competing interests:** None declared. **Data and materials availability:** RNA-seq data are deposited in GEO (accession number GSE120161) and can be visualized at https://devneuro.org/cdn/synapdomain.php. All data needed to evaluate the conclusions in the paper are present in the paper or the supplementary materials.

SUPPLEMENTARY MATERIALS

www.sciencemag.org/content/363/6425/413/suppl/DC1
Materials and Methods
Figs. S1 to S22
Tables S1 to S4
References (*31–58*)

25 July 2018; accepted 19 December 2018
10.1126/science.aau8977